SCIENTIFIC REPORTS

OPEN

CONFERENCE PROCEEDINGS

ACSMS2014

SUBJECT AREAS:
NANOPARTICLES
CATALYST SYNTHESIS
ELECTROCATALYSIS

Received
28 August 2014

Accepted
4 November 2014

Published
6 January 2015

Correspondence and requests for materials should be addressed to Y.Y. (bityanyiming@163.com); K.S. (bitkeningsun@163.com) or G.W. (Guoxiu.Wang@uts.edu.au)

Graphene-Co_3O_4 nanocomposite as electrocatalyst with high performance for oxygen evolution reaction

Yufei Zhao[1,2], Shuangqiang Chen[1], Bing Sun[1], Dawei Su[1], Xiaodan Huang[1], Hao Liu[1], Yiming Yan[2], Kening Sun[2] & Guoxiu Wang[1]

[1]Center for Clean Energy Technology, School of Chemistry and Forensic Science, Faculty of Science, University of Technology, Sydney, Sydney, NSW 2007, Australia, [2]Beijing Key Laboratory for Chemical Power Source and Green Catalysis, School of Chemical Engineering and Environment, Beijing Institute of Technology, Beijing, 100081, China.

Graphene-Co_3O_4 composite with a unique sandwich-architecture was successfully synthesized and applied as an efficient electrocatalyst for oxygen evolution reaction. Field emission scanning electron microscopy (FESEM) and transmission electron microscopy (TEM) analyses confirmed that Co_3O_4 nanocrystals were homogeneously distributed on both sides of graphene nanosheets. The obtained composite shows enhanced catalytic activities in both alkaline and neutral electrolytes. The onset potential towards the oxygen evolution reaction is 0.406 V (*vs.* Ag/AgCl) in 1 M KOH solution, and 0.858 V (*vs.* Ag/AgCl) in neutral phosphate buffer solution (PBS), respectively. The current density of 10 mA/cm^2 has been achieved at the overpotential of 313 mV in 1 M KOH and 498 mV in PBS. The graphene-Co_3O_4 composite also exhibited an excellent stability in both alkaline and neutral electrolytes. In particular, no obvious current density decay was observed after 10 hours testing in alkaline solution and the morphology of the material was well maintained, which could be ascribed to the synergistic effect of combining Co_3O_4 and graphene.

Solar-driven electrochemical transformation of small molecules, such as water splitting and carbon dioxide reduction, is one of the most promising approaches for producing clean and sustainable energy[1,2]. Photoelectrocatalytic or electrocatalytic water splitting is a process including water oxidation and reduction[3–6]. However, water splitting is mainly hindered by the oxygen evolution reaction (OER, $4H^+/4e^-$), which has several steps and requires large overpotential[7]. Currently, some noble metals (ruthenium and iridium) and their compounds exhibit excellent activity towards OER with low overpotential and high current density[8,9]. However, their application are hindered by the scarcity and high cost. Therefore, discovering efficient and inexpensive catalysts is critical to enhance the OER current density and reduce the overpotential.

In the past few years, considerable efforts have been dedicated to utilizing the earth-abundant metal oxides such as cobalt oxide[10–13] nickel oxide[14–16] and manganese oxide[17,18] materials, as electrocatalysts for OER. Among these catalysts, Co_3O_4 has attracted extensive attentions owing to its high activity and superior stability[12,19–21]. For example, mesoporous Co_3O_4 has been reported as the OER catalyst with current densities of 27.2 mA/cm^2 at 1 V (*vs.* Ag/AgCl) and the crystalline Co_3O_4 showed a relatively small Tafel slope (49 mV/decade)[19,20]. In addition, Co_3O_4 could also be utilized in photocatalytic system. Jiao *et al.* reported the photocatalytic properties of the mesoporous Co_3O_4 combined with the $[Ru(bpy)_3]^{2+}$ with a high turnover frequency (TOF) of $\sim 2.2 \times 10^{-3}$ s^{-1} per Co atom[22]. However, the strong causticity of alkaline solution and the intrinsically low conductivity of Co_3O_4 have impeded the further development of Co_3O_4 as OER catalyst.

Combining Co_3O_4 nanoparticles with conductive substrates can efficiently enhance the conductivity of the catalyst and significantly affect its catalytic activity and stability. Carbon materials, such as carbon nanotube (CNT), graphene (G) and mesoporous carbon, have been widely employed as the supporting substrates owing to their high conductivity and large specific surface area[23–26]. Recently, Dai's group synthesized Co_3O_4 nanocrystals supported on graphene by hydrothermal reaction and demonstrated high electrocatalytic performance[27]. Zhao and coworkers reported OER catalysts of Co_3O_4 nanoparticle/graphene composites, fabricated by the layer-by-layer assembly[28]. Co_3O_4/CNT (single-walled or multi-walled) materials were also prepared as high performance catalysts towards oxygen evolution[29,30].

Herein, we report a simple method to prepare a unique sandwich-architectured catalyst composed of graphene and Co_3O_4 (G-Co_3O_4). Ultrafine Co_3O_4 particles uniformly anchor onto both sides of graphene sheets. The unique sandwich-architecture leads to large amount loading of the active Co_3O_4 nanocrystals and enhances electron transfer kinetics between the materials. Therefore, the catalytic activity and stability of the catalyst have been substantially promoted. G-Co_3O_4 composite catalyst shows low overpotentials of 313 mV and 498 mV to achieve the current density of 10 mA/cm^2 in the alkaline and neutral conditions, respectively. Furthermore, there is no obvious current density decay after the stability test.

Results

Synthesis of G-Co_3O_4 nanocomposite. The synthesis of the sandwich-architectured composite is illustrated in Fig. 1. Cobalt (II) acetate was added into the xylene and oleic acid mixed solution. The oleic acid in the mixture acted as a capping agent in order to control the particle growth and prevent colloidal particles from aggregation. Then, the as-prepared GO solution was introduced into the above solution under vigorous stirring. Co^{II} cations attached on both sides of the GO nanosheets by electrostatic interaction[31]. During the following refluxing process and the reducing process by adding $NaBH_4$, Co nanoparticles were loaded on the surface of rGO nanosheets. The final product of G-Co_3O_4 with unique sandwich-architecture was obtained after calcination.

The characterization of the G-Co_3O_4 composite. The morphology of the precursor obtained after filtration and calcination in argon atmosphere was characterized by scanning electron microscopy (SEM, see Supplementary Fig. S1 online), which highly maintained the layer structure of graphene oxide. The morphology of the synthesized G-Co_3O_4 composite was investigated by SEM. The low magnification image in Fig. 2a clearly shows that the obtained G-Co_3O_4 composite still displayed layer structure, which is similar to the pristine graphene (see Supplementary Fig. S2a online). The high magnification in the inset of Fig. 2a shows two layers of Co_3O_4 particles homogeneously distributed. From the layer structure and the homogeneous distribution of the Co_3O_4 particles, we infer that the Co_3O_4 particles attached on both sides of the graphene nanosheets, which could form a unique sandwich-architecture. However, it is difficult to clearly find graphene because of the low content (8.8 wt.%, see Supplementary Fig. S3 online). The transmission electron microscopy (TEM) image in Fig. 2b further demonstrates the homogeneous distribution of Co_3O_4 nanoparticles on graphene substrate. High resolution TEM (HRTEM) in Fig. 2c clearly confirmed the sandwich-architecture. The graphene was definitely imbedded between the parallel layers of Co_3O_4 particles even after a strong sonication, suggesting a relatively strong interaction between graphene and Co_3O_4 particles. The graphene nanosheets acted as a binder to link neighboring Co_3O_4 particles together and also increased the conductivity of the composite. They can further prevent the aggregation of the Co_3O_4 nanoparticles during thermal treatment. We also synthesized pristine Co_3O_4 through similar process without adding graphene oxide. The SEM image (see Supplementary Fig. S2b online) shows the particle size of pristine Co_3O_4 is much bigger than that in G-Co_3O_4 composite. Furthermore, as shown in Figure 2d, the lattice fringes in HRTEM image and the selected area electron diffraction (SAED) pattern further confirmed the formation of crystalline Co_3O_4.

The crystal structure of the obtained G-Co_3O_4 composite and pristine Co_3O_4 nanoparticles was determined by X-ray diffraction (XRD) method as shown in Fig. 3a. The prominent peaks at 31.2, 37.1, 45.1, 59.7, 65.6° of G-Co_3O_4 and pristine Co_3O_4 can be indexed to face-centered cubic phase (Fd3m, JCPDS card No. 76-1802). The broad diffraction peak appeared at around 24.8° in the G-Co_3O_4

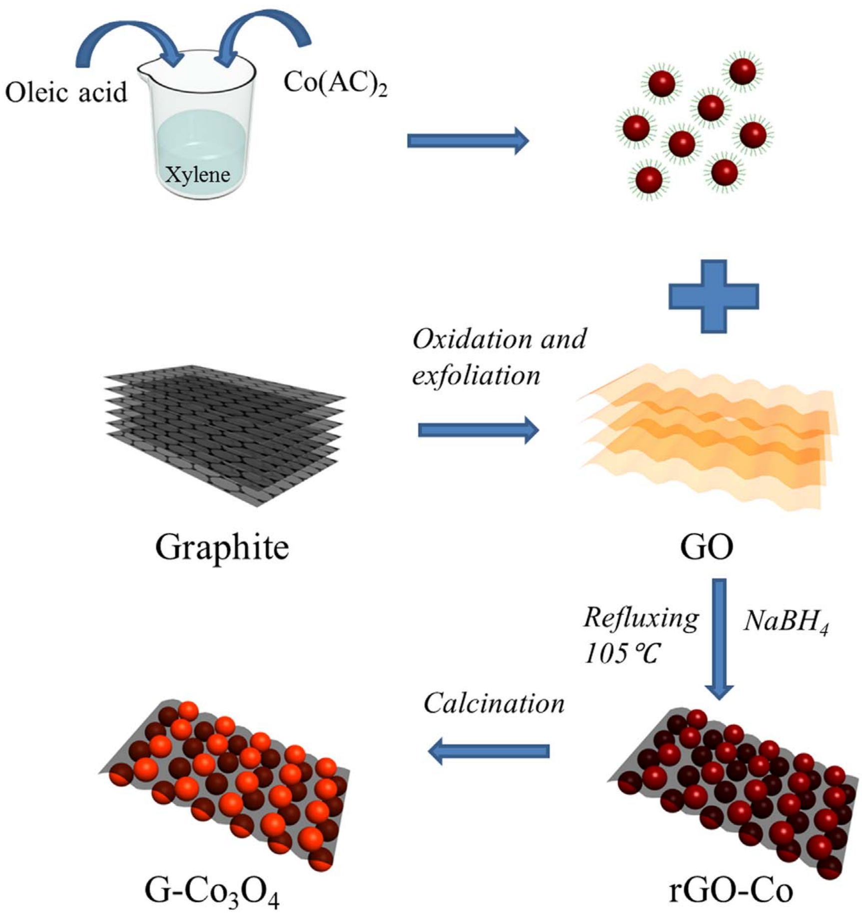

Figure 1 | **A schematic illustration for preparing G-Co_3O_4 nanocomposite with a sandwich-architecture.**

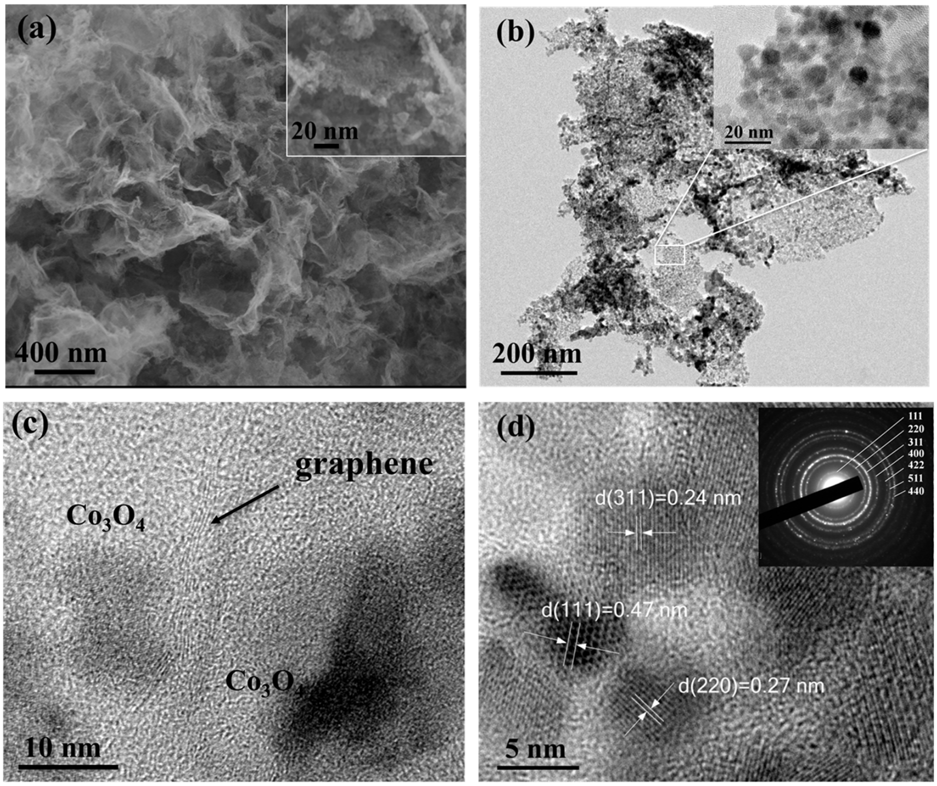

Figure 2 | Microscope observation of the G-Co_3O_4 composite. (a) Low and high magnification SEM images of G-Co_3O_4. (b) Low magnification TEM image of G-Co_3O_4. (c) High resolution TEM (HRTEM) image of G-Co_3O_4, showing a sandwich-like microstructure. (d) HRTEM image of Co_3O_4 nanocrystals and SAED pattern of G-Co_3O_4.

composite is attributed to the (002) direction of graphene. Raman spectra of the G-Co_3O_4 composite and pristine Co_3O_4 are shown in Fig. 3b. Two peaks at ca. 470 and 671 cm^{-1} can be assigned to Co_3O_4. Moreover, G-Co_3O_4 also displays another two obvious peaks at 1327 and 1584 cm^{-1}, which can be indexed to the peaks of graphene[32,33]. The XRD and Raman spectra further confirm the successful synthesis of G-Co_3O_4 composite catalyst.

Electrochemical performance of the OER catalyst. The water oxidation catalytic activities of the as-synthesized nanocomposite were first investigated in alkaline solution (0.1 or 1 M KOH) in a standard three-electrode setup. During the electrochemical test, the working electrode was continuously rotating at 1600 rpm to remove the generated oxygen bubbles. Linear sweep voltammetry (LSV) curves of G-Co_3O_4 catalysts are shown in Fig. 4a. Ruthenium nanocrystal functionalized carbon black catalysts (30% Ru loaded on carbon black, Ru/C) was also tested for comparison. G-Co_3O_4 catalyst exhibits significantly higher anodic current and lower onset potential than that of the Ru/C catalysts, in both 0.1 and 1 M KOH solutions (Fig. 4a). In 1 M KOH solution, G-Co_3O_4 catalyst shows a sharp onset potential at 0.406 V (*vs.* Ag/AgCl, following the method described by Chen et al.)[34], and achieves the current density of j = 10 mA/cm^2 at the overpotential of 313 mV, which is much better than that of the Co_3O_4/SWNTs (593 mV) and mesoporous Co_3O_4 catalysts (525 mV) in the same alkaline solution, and even comparable to the best performance of G/Co_3O_4 catalysts (310 mV)[20,27,29]. In 0.1 M KOH, G-Co_3O_4 catalyst also exhibits a lower onset catalytic potential (0.446 V *vs.* Ag/AgCl) and higher current density (achieved a current density of j = 10 mA/cm^2 at the overpotential of 359 mV) than those of the Ru/C catalyst.

Based on the mass content of the Co_3O_4 in the composite calculated from the TGA test and assuming that all deposited materials were involved in the electrochemical reaction, the lower limits for turnover frequency (TOF) can be derived from the catalytic current.

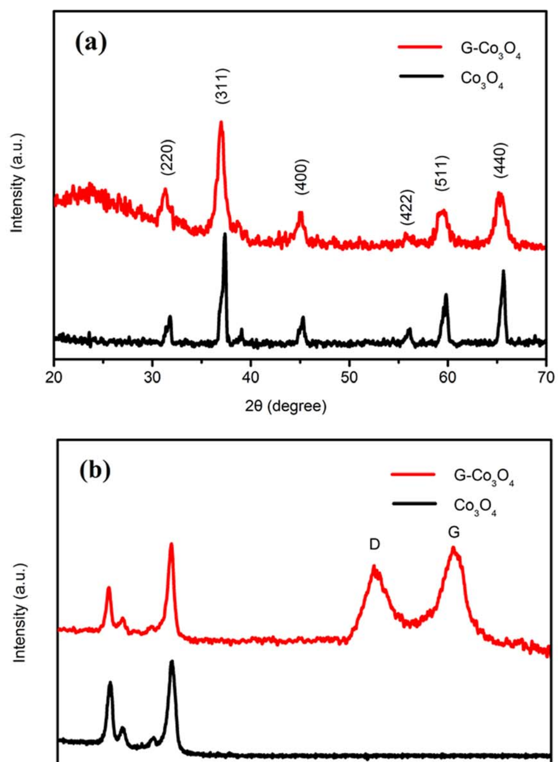

Figure 3 | The characterization of the G-Co_3O_4 composite. (a) XRD patterns of Co_3O_4 and G-Co_3O_4 composite. (b) Raman spectra of Co_3O_4 and G-Co_3O_4 composite catalyst.

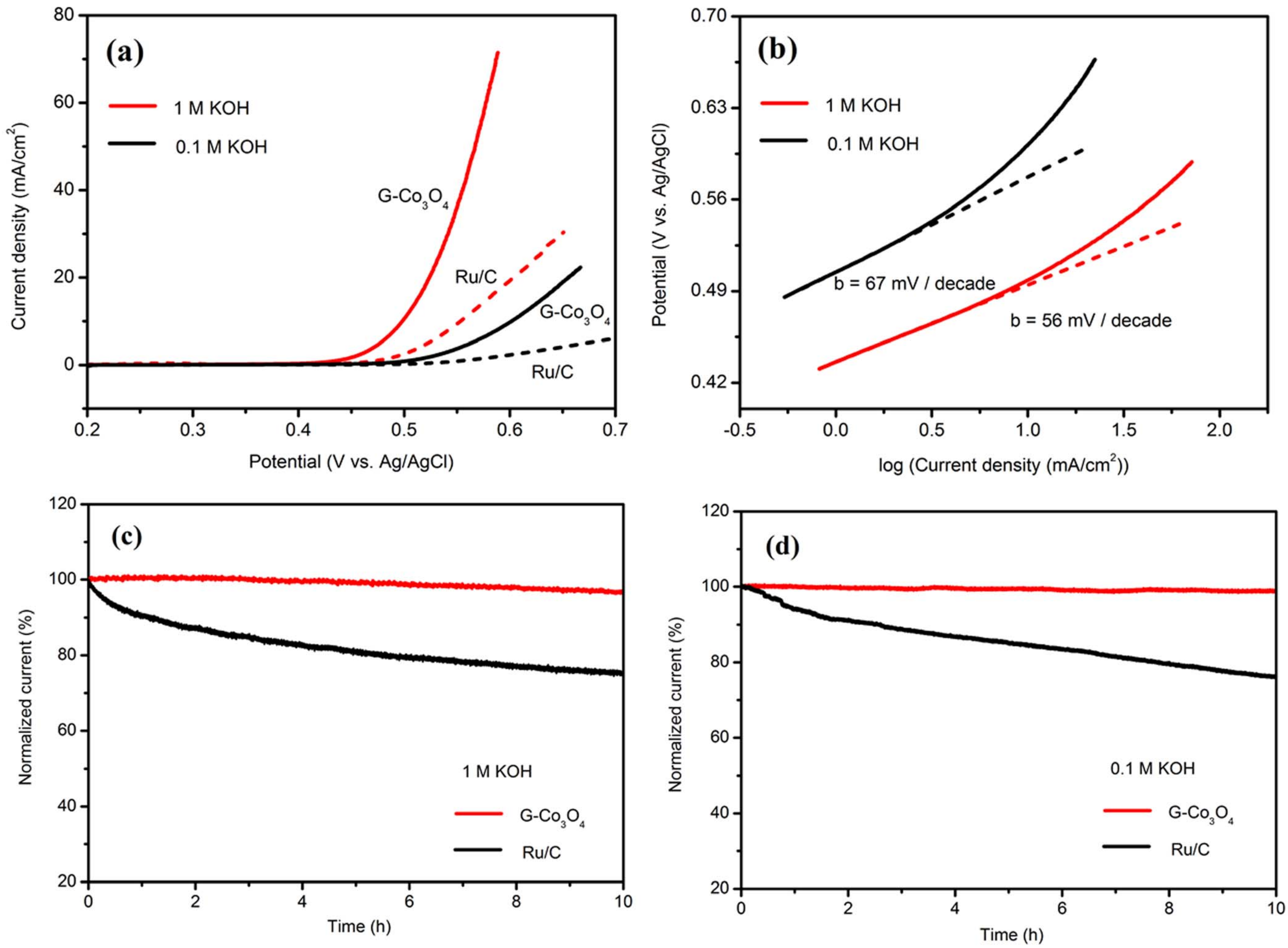

Figure 4 | Electrochemical performance. (a) Polarization curves of G-Co_3O_4 and Ru/C catalysts on GC electrodes in 0.1 and 1 M KOH. (b) The Tafel curves of G-Co_3O_4 in 0.1 and 1 M KOH. (c, d) Chronoamperometric responses (percentage of current retained versus operation time) of G-Co_3O_4 and Ru/C catalysts in 1 M and 0.1 M KOH electrolytes.

We calculated a high TOF of 0.45 s^{-1} referring to per Co atom for G-Co_3O_4 catalyst at the overpotential of 350 mV in 1 M KOH and 0.194 s^{-1} at the overpotential of 400 mV in 0.1 M KOH, which are higher than those of previous reports about Co based materials (Co_3O_4, 0.08 s^{-1} at overpotential of 507 mV in 1 M KOH and mesoporous Co_3O_4, 3.16×10^{-3} s^{-1} at 400 mV in 0.1 M KOH)[10,20].

Tafel plot is applied to evaluate the efficiency of the catalytic reaction in alkaline solutions (0.1 and 1 M KOH), which is derived from the polarization curves using the Tafel equation $\eta = b \log(j/j_0)$, where η is the overpotential, b is the Tafel slope, j is the current density, and j_0 is the exchange current density. The G-Co_3O_4 catalyst exhibits Tafel slopes of b = 56 mV/decade in 1 M KOH and b = 67 mV/decade in 0.1 M KOH (Fig. 4b), which are lower than previously reported G/Co_3O_4 (67 mV/decade in 1 M KOH) and graphene/$NiCo_2O_4$ hybrid paper (156 mV/decade in 0.1 M KOH)[27,35]. The observed Tafel slope value suggests the favorable OER kinetics over G-Co_3O_4 catalyst and also the good chemical and electronic coupling between the Co_3O_4 nanoparticles and graphene nanosheets.

The G-Co_3O_4 catalyst also exhibits good stability in the alkaline solutions, which is another important factor for energy conversion systems. In 1 M KOH solution, the G-Co_3O_4 electrode shows excellent durability with no obvious activity decay compared with the initial value, while the Ru/C catalyst electrode degrades by 25.8% of the initial value (Fig. 4c). A similar trend is also observed in 0.1 M KOH (Fig. 4d). The result of repeating potential cycling for 1000 cycles also confirmed the good stability of the material. After cycling test, the polarization curve of the G-Co_3O_4 modified electrode was almost the same as the initial one (see Supplementary Fig. S4 online). Furthermore, no obvious morphology change is observed in the SEM image of G-Co_3O_4 after long-term stability testing (see Supplementary Fig. S5 online), suggesting that G-Co_3O_4 catalyst can tolerate long-term corrosion and possess robust mechanical properties.

The G-Co_3O_4 composite has shown high catalytic activity and good stability towards OER in alkaline solution. On the other hand, the enhanced catalytic activities in neutral solution are more desirable owing to the benign nature and weak causticity. The catalytic activity of Co_3O_4 towards OER is sensitive to a low pH value, especially for the neutral solution according to the previous investigation[36]. Therefore, it is necessary to evaluate the electrochemical performance of G-Co_3O_4 catalyst in neutral solution. The G-Co_3O_4 electrode with the same mass loading was tested in 0.1 M phosphate buffer solution (PBS) at pH 7. The LSV curve of G-Co_3O_4 catalyst and the corresponding Tafel plot obtained in the neutral solution are presented in Fig. 5a. In the neutral condition, G-Co_3O_4 catalyst shows an onset potential at 0.858 V (*vs.* Ag/AgCl) and achieves a current density of $j = 10$ mA/cm^2 at the overpotential of 498 mV, which exhibit better performance than those of the previous report (810 mV)[29]. Moreover, G-Co_3O_4 catalyst exhibits a little smaller Tafel plot of 98 mV/decade compared to others (104 mV/decade or 110 mV/decade)[29,37]. The decreased Tafel slope value can

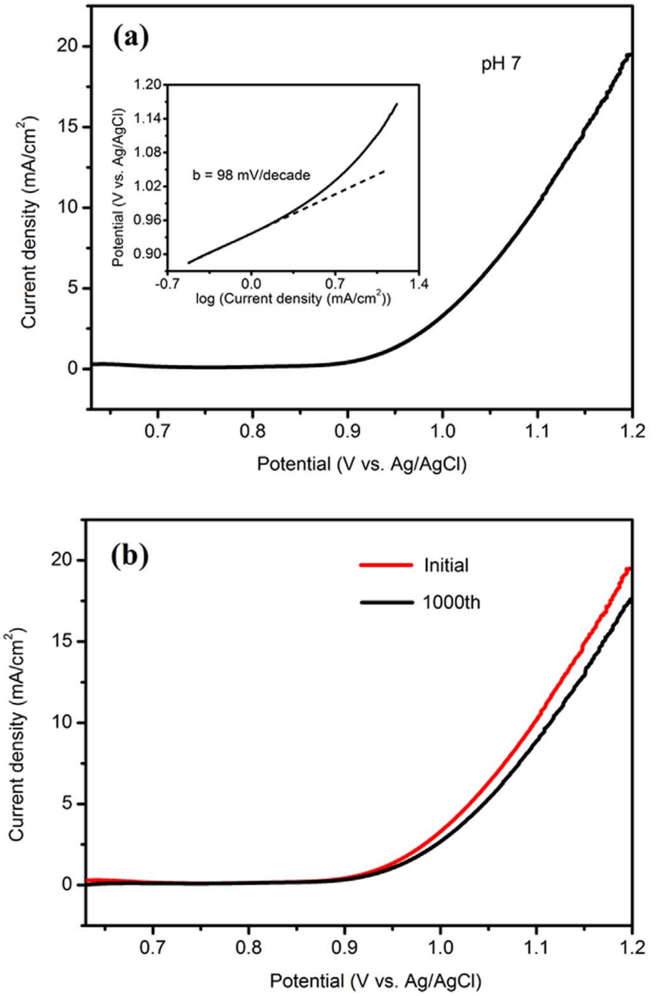

Figure 5 | Electrochemical performance of G-Co_3O_4 composite OER catalyst. (a) LSV and Tafel slope of G-Co_3O_4 in neutral solution, (b) OER stability test of G-Co_3O_4, the initial and 1000th polarization curves in neutral solution.

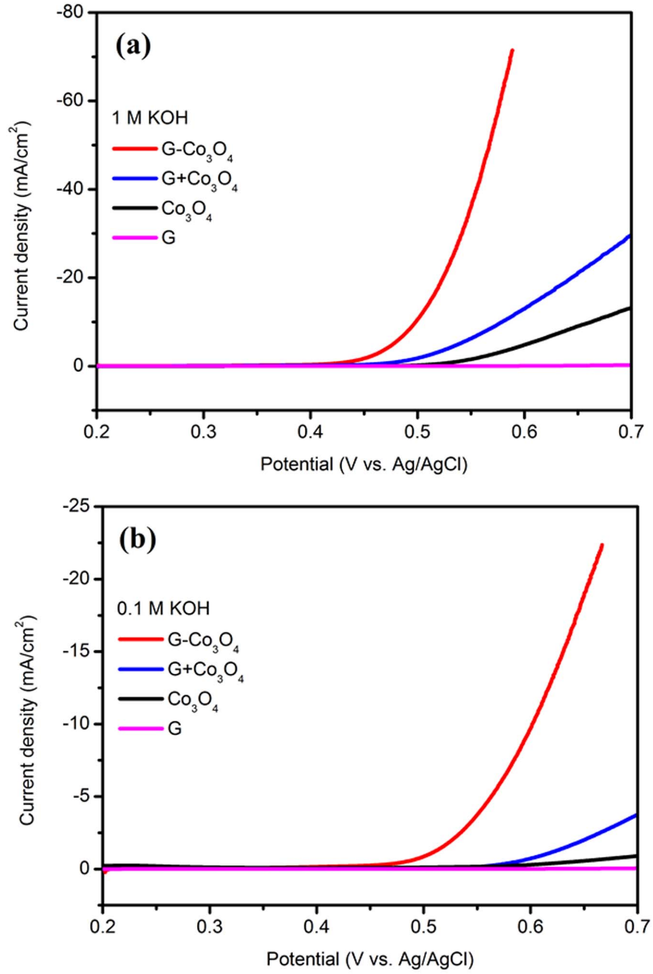

Figure 6 | Electrochemical performance. Polarization curves of G-Co_3O_4, G+Co_3O_4, the pristine Co_3O_4 and graphene in (a) 1 M and (b) 0.1 M KOH solutions.

be ascribed to the synergistic coupling and the fast charge transport of the materials. Furthermore, the stability of G-Co_3O_4 is assessed by repeated potential cycling for 1000 cycles, as shown in Fig. 5b. Only a slight decay of the activity (<10%) was observed referred to the polarization curves after the long-term test.

Discussion

The excellent electrochemical performance of G-Co_3O_4 catalyst suggests its promising application towards OER both in alkaline and neutral solution. The high activity and excellent durability of G-Co_3O_4 towards OER are mainly attributed to the unique sandwich-architecture of the materials. A series of controlled experiments, shown in Fig. 6, have demonstrated that the obtained G-Co_3O_4 catalyst displayed better OER activity than those of the simple physical mixture of Co_3O_4 and graphene (G+Co_3O_4), pure Co_3O_4 and graphene in 1 M and 0.1 M KOH conditions. The activity order is G-Co_3O_4 > G+Co_3O_4 > pure Co_3O_4 > graphene. The strong interaction of Co_3O_4 nanoparticles with graphene nanosheets and the unique sandwich-architecture have strong effect on the catalytic property of the composite. Simple physical mixing cannot create effective interfacial contacts between the Co_3O_4 nanoparticles and graphene nanosheets. This was also confirmed by the electrochemical impedance spectroscopy (see Supplementary Fig. S6 online). The Nyquist plots showed that the OER charge resistance of the G-Co_3O_4 catalyst is the smallest among the other samples (G+Co_3O_4, Co_3O_4). This further illustrates that the strong chemical coupling and good interaction between the Co_3O_4 and graphene can significantly improve the electron transport and reaction kinetics during the OER. In order to further investigate the high performance of G-Co_3O_4, the effective surface areas were estimated, which was determined by electrochemical capacitance measurements from static cyclic voltammetry (see Supplementary Fig. S7 online)[38,39]. The capacitance for G-Co_3O_4 composite is 12.4 mF/cm^2, which is much higher than G+Co_3O_4 (2.8 mF/cm^2). Therefore, the high performance could be also associated with the high electroactive surface area.

The observed enhanced activity of the G-Co_3O_4 catalyst indicates that the sandwich-architecture is favorable for the oxygen evolution, in which the graphene nanosheets provide large specific surface area and good conductivity. This specific structure also leads to large amount loading and much small particle size of the Co_3O_4 anchored on both sides of the graphene sheets, which provides much more electroactive surface area for the oxygen evolution. In addition, the unique and intimate contact between the graphene and Co_3O_4 afforded by one-step facile mechanism contributes to the superior catalytic activity.

In conclusion, sandwich-architectured G-Co_3O_4 composite was successfully synthesized exhibiting good interaction between Co_3O_4 nanoparticles and graphene nanosheets. G-Co_3O_4 catalyst exhibits enhanced catalytic performances with high catalytic activities, good stability and favorable reaction kinetics in both the alkaline and neutral solutions, as catalyst for water oxidation. The enhanced catalytic performance demonstrates large electroactive surface area, fast electron transfer rate and superior electrical and chemical coupling of the composite. The unique morphology and excellent electrochemical performance of G-Co_3O_4 catalyst render this material a promising noble metal free catalyst towards the oxygen evolution reaction.

Methods

Materials synthesis. Graphene oxide (GO) was prepared by the oxidation and exfoliation of the graphite according to the previously reported procedure[40,41]. Sandwich-like G-Co_3O_4 was synthesized *via* an oleic acid assisted method followed by thermal treatment[42]. In a typical synthesis process, 0.68 g oleic acid was mixed with 40 mL dry xylene under vigorous magnetic stirring. Then, 0.5 g cobalt acetate tetrahydrate ($Co(AC)_2$, Aldrich) was introduced into the mixture and sonicated for 1 min. After that, the mixture was mixed with 40 ml GO solution (2 mg ml^{-1}) by vigorous stirring and reacted in a pre-heated oil bath under refluxing for 4 h at 105°C. Then, 10 ml (5 mg/ml) $NaBH_4$ was added to the reaction mixture and kept stirring for another 10 min. The precipitation was collected by filtration and annealed at 300°C for 3 h in argon atmosphere. The final product was obtained after annealing at 400°C for another 2 h in air. The pristine Co_3O_4 was synthesized by similar method without the addition of GO solution. The comparision sample of ruthenium nanocrystals supported on carbon black (Ru/C) was synthesized by using hydrophilic and hydrophobic tri-block copolymer F127 as a soft template, followed by low temperature heat treatment[43].

Structural characterization. The morphology of the obtained materials was characterized by field emission scanning electron microscopy (FESEM, Zeiss Supra 55VP) and transmission electron microscopy (TEM, Model JEM-2011, JEOL). X-ray diffraction (XRD) patterns were collected on Siemens D5000 diffractometer using Cu Kα radiation with a scanning step of 0.02° per second. Raman spectra were recorded with an inVia Renishaw Raman spectrometer system (HR Micro Raman spectrometer, Horiba JOBIN YVON US/HR800 UV) equipped with a 632.8 nm wavelength laser. Thermal gravimetric analysis (TGA) of G-Co_3O_4 composite was performed using a TGA/differential thermal analysis (DTA) analyzer (TA Instruments, SDT 2960 module, New Castle, DE, USA) at a heating rate of 10°C min^{-1} in air from room temperature to 700°C.

Electrochemical measurements. Electrocatalytic activity measurements were carried out on an electrochemical workstation (CHI 660E) in a three-electrode glass cell system. A glass carbon (GC) electrode coated with as-prepared materials was used as the working electrode. A platinum wire was used as the counter electrode (CE). The potential was recorded using an Ag/AgCl (1 M KCl) reference electrode, which was converted to the reversible hydrogen electrode (RHE) according to Nernst equation $E_{RHE} = E_{Ag/AgCl} + 0.059 \times pH + 0.2224$. The working electrode was prepared as follows: 4 mg sample was dispersed in 1 ml of 1 : 1 v/v water/isopropanol by ultrasonication. Then 80 μl Nafion (5 wt%) was added to the solution to obtain a homogeneous ink. The catalyst ink (10 μl) was loaded onto the GC electrode with a diameter of 5 mm. LSV was conducted in KOH solution (0.1 M, 1 M) and phosphate buffer solution (PBS, 0.1 M) at a scan rate of 2 mV s^{-1}. The polarization curves were all corrected by 95% iR compensation and our typical electrochemical cell had $R_u = \sim 8\ \Omega$ in 1 M KOH, $R_u = \sim 20\ \Omega$ in 0.1 M KOH and $R_u = \sim 26\ \Omega$ in 0.1 M PBS. TOFs were calculated according to the equation of $TOF = n_{O2}/n_{Co} = (Q/4F)/n_{Co}$ (F is the faraday constant, 96485 C/mol). Stability was carried out for 10 h at 0.50 V (*vs.* Ag/AgCl) in 1 M KOH and 0.60 V (*vs.* Ag/AgCl) in 0.1 M KOH solution. Electrical impedance spectroscopy (EIS) was recorded under the following condition: ac voltage amplitude 5 mV, frequency ranges from 10^6 to 0.1 Hz, and open circuit. Cyclic voltammograms (CV) of G-Co_3O_4 and G+Co_3O_4 measured in 1 M KOH solution in a potential window (−0.16 V to −0.08 V (*vs.* Ag/AgCl)) without faradaic processes with scan rates of 10, 30, 50, 70, 90 mV/s.

1. Haussener, S., Hu, S., Xiang, C. X., Weber, A. Z. & Lewis, N. S. Simulations of the irradiation and temperature dependence of the efficiency of tandem photoelectrochemical water-splitting systems. *Energy. Environ. Sci.* **6**, 3605–3618 (2013).
2. Kondratenko, E. V., Mul, G., Baltrusaitis, J., Larrazabal, G. O. & Perez-Ramirez, J. Status and perspectives of CO_2 conversion into fuels and chemicals by catalytic, photocatalytic and electrocatalytic processes. *Energy. Environ. Sci.* **6**, 3112–3135 (2013).
3. Zhang, Z. H. *et al.* Carbon-Layer-Protected Cuprous Oxide Nanowire Arrays for Efficient Water Reduction. *Acs Nano* **7**, 1709–1717 (2013).
4. Zhao, Y. F., Zhang, Y. X., Yang, Z. Y., Yan, Y. M. & Sun, K. N. Synthesis of MoS_2 and MoO_2 for their applications in H-2 generation and lithium ion batteries: a review. *Sci. Technol. Adv. Mater.* **14**, 12pp (2013).
5. Voiry, D. *et al.* Enhanced catalytic activity in strained chemically exfoliated WS_2 nanosheets for hydrogen evolution. *Nat. Mater.* **12**, 850–855 (2013).
6. Li, Y. G., Hasin, P. & Wu, Y. Y. $Ni_xCo_{3-x}O_4$ Nanowire Arrays for Electrocatalytic Oxygen Evolution. *Adv. Mater.* **22**, 1926–+ (2010).
7. Meyer, T. J. Catalysis - The art of splitting water. *Nature* **451**, 778–779 (2008).
8. Fillol, J. L. *et al.* Efficient water oxidation catalysts based on readily available iron coordination complexes. *Nat. Chem.* **3**, 807–813 (2011).
9. Lewis, N. S. & Nocera, D. G. Powering the planet: Chemical challenges in solar energy utilization. *Proc. Natl. Acad. Sci.* **103**, 15729–15735 (2006).
10. Chou, N. H., Ross, P. N., Bell, A. T. & Tilley, T. D. Comparison of Cobalt-based Nanoparticles as Electrocatalysts for Water Oxidation. *Chemsuschem* **4**, 1566–1569 (2011).
11. Zou, X. X. *et al.* Efficient oxygen evolution reaction catalyzed by low-density Ni-doped Co_3O_4 nanomaterials derived from metal-embedded graphitic C_3N_4. *Chem. Comm.* **49**, 7522–7524 (2013).
12. Wang, D. D., Chen, X., Evans, D. G. & Yang, W. S. Well-dispersed Co_3O_4/Co_2MnO_4 nanocomposites as a synergistic bifunctional catalyst for oxygen reduction and oxygen evolution reactions. *Nanoscale* **5**, 5312–5315 (2013).
13. Lu, B. A., Cao, D. X., Wang, P., Wang, G. L. & Gao, Y. Y. Oxygen evolution reaction on Ni-substituted Co_3O_4 nanowire array electrodes. *Int. J. Hydrogen Energy* **36**, 72–78 (2011).
14. Dinca, M., Surendranath, Y. & Nocera, D. G. Nickel-borate oxygen-evolving catalyst that functions under benign conditions. *Proc. Natl. Acad. Sci.* **107**, 10337–10341 (2010).
15. Zhou, W. J. *et al.* Ni_3S_2 nanorods/Ni foam composite electrode with low overpotential for electrocatalytic oxygen evolution. *Energy. Environ. Sci.* **6**, 2921–2924 (2013).
16. Gong, M. *et al.* An Advanced Ni-Fe Layered Double Hydroxide Electrocatalyst for Water Oxidation. *J. Am. Chem. Soc.* **135**, 8452–8455 (2013).
17. Jiao, F. & Frei, H. Nanostructured cobalt and manganese oxide clusters as efficient water oxidation catalysts. *Energy. Environ. Sci.* **3**, 1018–1027 (2010).
18. Zaharieva, I. *et al.* Synthetic manganese-calcium oxides mimic the water-oxidizing complex of photosynthesis functionally and structurally. *Energy. Environ. Sci.* **4**, 2400–2408 (2011).
19. Koza, J. A., He, Z., Miller, A. S. & Switzer, J. A. Electrodeposition of Crystalline Co_3O_4-A Catalyst for the Oxygen Evolution Reaction. *Chem. Mater.* **24**, 3567–3573 (2012).
20. Tuysuz, H., Hwang, Y. J., Khan, S. B., Asiri, A. M. & Yang, P. D. Mesoporous Co_3O_4 as an electrocatalyst for water oxidation. *Nano. Res.* **6**, 47–54 (2013).
21. Esswein, A. J., McMurdo, M. J., Ross, P. N., Bell, A. T. & Tilley, T. D. Size-Dependent Activity of Co_3O_4 Nanoparticle Anodes for Alkaline Water Electrolysis. *J. Phys. Chem. C* **113**, 15068–15072 (2009).
22. Rosen, J., Hutchings, G. S. & Jiao, F. Ordered Mesoporous Cobalt Oxide as Highly Efficient Oxygen Evolution Catalyst. *J. Am. Chem. Soc.* **135**, 4516–4521 (2013).
23. Mu, Y. Y., Liang, H. P., Hu, J. S., Jiang, L. & Wan, L. J. Controllable Pt nanoparticle deposition on carbon nanotubes as an anode catalyst for direct methanol fuel cells. *J. Phys. Chem. B* **109**, 22212–22216 (2005).
24. Liu, Q., Jin, J. T. & Zhang, J. Y. $NiCo_2S_4$@graphene as a Bifunctional Electrocatalyst for Oxygen Reduction and Evolution Reactions. *ACS Appl. Mater. Interfaces* **5**, 5002–5008 (2013).
25. Liang, Y. Y. *et al.* Covalent Hybrid of Spinel Manganese-Cobalt Oxide and Graphene as Advanced Oxygen Reduction Electrocatalysts. *J. Am. Chem. Soc.* **134**, 3517–3523 (2012).
26. Bian, X. J. *et al.* Nanocomposite of MoS_2 on ordered mesoporous carbon nanospheres: A highly active catalyst for electrochemical hydrogen evolution. *Electrochem. Commun.* **22**, 128–132 (2012).
27. Liang, Y. Y. *et al.* Co_3O_4 nanocrystals on graphene as a synergistic catalyst for oxygen reduction reaction. *Nat. Mater.* **10**, 780–786 (2011).
28. Suryanto, B. H. R., Lu, X. Y. & Zhao, C. Layer-by-layer assembly of transparent amorphous Co_3O_4 nanoparticles/graphene composite electrodes for sustained oxygen evolution reaction. *J. Mater. Chem. A* **1**, 12726–12731 (2013).
29. Wu, J. *et al.* Co_3O_4 nanocrystals on single-walled carbon nanotubes as a highly efficient oxygen-evolving catalyst. *Nano. Res.* **5**, 521–530 (2012).
30. Lu, X. Y. & Zhao, C. Highly efficient and robust oxygen evolution catalysts achieved by anchoring nanocrystalline cobalt oxides onto mildly oxidized multiwalled carbon nanotubes. *J. Mater. Chem. A* **1**, 12053–12059 (2013).
31. Yang, P. D., Zhao, D. Y., Margolese, D. I., Chmelka, B. F. & Stucky, G. D. Generalized syntheses of large-pore mesoporous metal oxides with semicrystalline frameworks. *Nature* **396**, 152–155 (1998).
32. Gao, M. R. *et al.* Nitrogen-Doped Graphene Supported $CoSe_2$ Nanobelt Composite Catalyst for Efficient Water Oxidation. *Acs Nano* **8**, 3970–3978 (2014).
33. Duan, J. J. *et al.* Mesoporous hybrid material composed of Mn_3O_4 nanoparticles on nitrogen-doped graphene for highly efficient oxygen reduction reaction. *Chem. Comm.* **49**, 7705–7707 (2013).
34. Chen, W. F. *et al.* Hydrogen-Evolution Catalysts Based on Non-Noble Metal Nickel-Molybdenum Nitride Nanosheets. *Angew. Chem. Int. Ed.* **51**, 6131–6135 (2012).
35. Chen, S. & Qiao, S. Z. Hierarchically Porous Nitrogen-Doped Graphene-$NiCo_2O_4$ Hybrid Paper as an Advanced Electrocatalytic Water-Splitting Material. *Acs Nano* **7**, 10190–10196 (2013).
36. Minguzzi, A., Fan, F. R. F., Vertova, A., Rondinini, S. & Bard, A. J. Dynamic potential-pH diagrams application to electrocatalysts for water oxidation. *Chem. Sci.* **3**, 217–229 (2012).
37. Nakagawa, T., Beasley, C. A. & Murray, R. W. Efficient Electro-Oxidation of Water near Its Reversible Potential by a Mesoporous IrO_x Nanoparticle Film. *J. Phys. Chem. C* **113**, 12958–12961 (2009).

38. Kong, D. S., Wang, H. T., Lu, Z. Y. & Cui, Y. $CoSe_2$ Nanoparticles Grown on Carbon Fiber Paper: An Efficient and Stable Electrocatalyst for Hydrogen Evolution Reaction. *J. Am. Chem. Soc.* **136**, 4897–4900 (2014).
39. McCrory, C. C. L., Jung, S. H., Peters, J. C. & Jaramillo, T. F. Benchmarking Heterogeneous Electrocatalysts for the Oxygen Evolution Reaction. *J. Am. Chem. Soc.* **135**, 16977–16987 (2013).
40. Yang, X. W., Zhu, J. W., Qiu, L. & Li, D. Bioinspired Effective Prevention of Restacking in Multilayered Graphene Films: Towards the Next Generation of High-Performance Supercapacitors. *Adv. Mater.* **23**, 2833–+ (2011).
41. Hummers, W. S. & Offeman, R. E. Preparation of Graphitic Oxide. *J. Am. Chem. Soc.* **80**, 1339–1339 (1958).
42. Lu, Y., Lu, X. M., Mayers, B. T., Herricks, T. & Xia, Y. N. Synthesis and characterization of magnetic Co nanoparticles: A comparison study of three different capping surfactants. *J. Solid State Chem.* **181**, 1530–1538 (2008).
43. Sun, B., Munroe, P. & Wang, G. X. Ruthenium nanocrystals as cathode catalysts for lithium-oxygen batteries with a superior performance. *Sci. Rep.* **3**, 2247; DOI:10.1038/srep02247 (2013).

Acknowledgments

This project is financially supported by the Australian Research Council (ARC) through the ARC Discovery project (DP1093855), ARC Future Fellowship project (FT110100800), the National Natural Science Foundation of China (Grant nos. 21175012, 21006015 and 21070623), Ministry of Science and Technology (2012DFR40240) and partially supported from the China Scholarship Council (CSC, No. 201306030039).

Author contributions

G.W. designed the experiments, co-wrote the manuscript. Y.Z. performed the major part of experiments, organized the data, and wrote the manuscript. D.S. contributed to the TEM experiments and discussion. S.C., B.S., X.H., K.S., Y.Y. and H.L. involved in discussion. All authors read and approved the final manuscript.

Additional information

Supplementary information accompanies this paper at http://www.nature.com/scientificreports

Competing financial interests: The authors declare no competing financial interests.

How to cite this article: Zhao, Y. *et al.* Graphene-Co_3O_4 nanocomposite as electrocatalyst with high performance for oxygen evolution reaction. *Sci. Rep.* **5**, 7629; DOI:10.1038/srep07629 (2015).